8.10 Inner-Core Dynamics

I. Sumita, Kanazawa University, Kanazawa, Japan

M. I. Bergman, Simon's Rock College, Great Barrington, MA, USA

8.10.1 Introduction

With a radius of 1200 km the Earth's inner core is only 30% smaller than its moon. Being the solid, central core of a planet, its dynamics are fascinating and unique. The inner-core boundary is a solid–liquid phase boundary, where the geotherm crosses the liquidus temperature of the iron alloy that comprises the Earth's core. The solidity of the inner core is a consequence of the melting temperature gradient being steeper than the geothermal gradient, as a result of the effects of pressure on the liquidus temperature. In smaller planets and satellites the entire core may be solid. As the Earth cools and solidification proceeds, the radius of the inner-core boundary increases with time. There is considerable uncertainty in the parameters required for thermal history calculations, but it is likely that the inner core is between 1 and 3 billion years old. Many of the dynamical processes that take place in the inner core are likely to be related to its growth, which in turn is strongly controlled by the pattern of heat transfer in the outer core, or in other words, the 'climate' of the outer core. Although the inner core, outer core, and mantle are all dynamically coupled, both thermally and mechanically, the effects of coupling are particularly important for the inner core because of its small volumetric size. This implies that the inner core can act as a recorder of the geodynamical processes occurring not only in the outer core, but also in the mantle.

The study of inner-core dynamics has been motivated by a wide range of observations and inferences, many coming from seismology. Geodynamics has attempted to explain the origin of these inner-core properties and attributes, such as elastic anisotropy

and anomalously high attenuation. Another set of observations that has given us insight into the inner core comes from geomagnetism. For example, inner-core solidification has been proposed to be an important candidate for the energy source to drive the geodynamo, and it may affect long-term variations of the strength of the geomagnetic dipole. In addition, motion of the inner core is thought to affect geodetic observations of polar motion.

In this chapter a review of current understanding of the dynamical processes that operate in the inner core is presented. First, a review of current knowledge of the composition of the inner core and its phase relations is presented. These are important for estimating the compositional buoyancy that helps drive convection in the outer core (*see* Chapters 8.02 and 8.05), and for understanding the process through which the inner core is solidifying. Next, a discussion on the grain size and stress in the inner core, which are important in controlling the mechanism and timescale of deformation and hence the strain rate and viscosity, is presented. This is followed by a critical examination of models proposed for the origin of inner core elastic anisotropy, one of the most intriguing features of the inner core. These models require knowledge of the stable phase of iron under inner-core conditions and the single-crystal elasticity of the hexagonal close-packed phase of iron, which remain uncertain. Also reviewed here is the orgin of other properties inferred of the inner core, such as anomalously high attenuation and lateral heterogeneity. Finally, the mechanisms of inner-core superrotation, another consequence of the dynamical coupling between the inner core and the outer core, are discussed.

8.10.2 Core Composition, Phase Diagram, and Crystal Structure of Iron

This section examines the composition and phase diagram of the core, in particular, how they impact the solidification and deformation of the Earth's inner core. We also examine briefly the crystal structure of iron under inner-core conditions. See Jeanloz (1990) and Poirier (1994) for detailed reviews on the composition of the core, and Boehler (1996a, 1996b) for a review of the pressure–temperature phase diagram of iron (evidence for the existence of the various solid phases and the variation of the melting temperature with pressure).

8.10.2.1 Composition of the Core

The composition of the core remains "an uncertain mixture of all the elements" (Birch, 1952). The average density of the Earth, the solar abundance of the elements, and the presence of iron meteorites, thought to be remnants of planetoid cores, all point to the core containing elemental iron (Birch, 1952). Comparison with iron meteorites (Brown and Patterson, 1948; Buchwald, 1975) suggests that the core also contains about 8% nickel by mass. Because nickel has a density similar to that of iron (Stacey, 1992), its presence in the core is difficult to detect seismically, and furthermore, little theoretical or experimental work on the partitioning of nickel has been carried out.

More studies have been aimed at the composition of the less-dense alloying components in the core, and their partitioning upon solidification. Early static compression experiments extrapolated to core conditions (Bridgman, 1949; Birch, 1952) and shock compression experiments (McQueen and Marsh, 1966) showed that iron–nickel alloys under core pressures are about 6–10% more dense than the outer core (Bullen, 1949), implying that less-dense alloying components must be present. Recent calculations using first principles and molecular dynamics (Laio *et al*., 2000) confirm that liquid iron at 330 GPa and 5400 K is about 6% more dense than the seismic Earth model PREM in the core (Dziewonski and Anderson, 1981), and calculations based on lattice potential theory lean toward a 10% deficit (Shanker *et al*., 2004.

Iron meteorites contain FeS (troilite) inclusions, suggesting that FeS may alloy with iron in the core (Mason, 1966), and experiments show that sulfur has an affinity for liquid iron–nickel alloys, at least in the range 2–25 GPa and 2073–2623 K (Li and Agee, 2001). Iron–sulfur–silicon liquids have been found to be miscible above 15 GPa at 2343 K (Sanloup and Fei, 2004). Cosmochemical arguments have been made that the mantle is depleted in sulfur relative to its chondritic abundance by two orders to magnitude, and that the missing sulfur could reside in the core (Murthy and Hall, 1970). However, since sulphur is volatile, this line of argument has been questioned (Ringwood, 1977).

FeO is absent from iron meteorites because at atmospheric pressure it is soluble by less than 0.1% by mass in solid iron, and its solubility increases only slightly above the liquidus (Ringwood, 1977). However, its solubility increases with temperature

and pressure as it becomes metallic, so that it could be present in the core (Ringwood and Hibberson, 1990). Other possible alloying components include iron silicate (Fe_xSi_{1-x}), Fe_3C, and FeH (MacDonald and Knopoff, 1958; Wood, 1993; Fukai, 1984; Okuchi, 1997; Lin *et al.*, 2002), all likely to be metallic under core pressures. Abundance and volatility during condensation from the nebula, the mode of core formation, and solubility in iron during core formation presumably determined the composition of less-dense elements in the core. See McDonough (2003) for a comprehensive discussion of light elements in the core.

The inner core is more dense than the outer core, by about $600\,kg\,m^{-3}$ according to the seismic Earth model PREM (Dziewonski and Anderson, 1981), and $550 \pm 50\,kg\,m^{-3}$ according to a model by Masters and Shearer (1990). Part of this difference, perhaps $200\,kg^{-3}$, can be attributed to iron being more dense in the solid phase (Stacey 1992; Laio, *et al.*, 2000). The rest is attributed to the less-dense alloying components partitioning into the outer core during solidification of the core. This partitioning has important consequences for the thermodynamics (*see* Chapter 8.02), fluid dynamics (*see* Chapter 8.05), and metallurgy of the core (see Section 8.10.3).

The seismically inferred density increase at the inner–outer core boundary, above that due to the phase transition, can be explained if the core is an iron-rich alloy. However, unless the solidus slope is vertical in a phase diagram, some nonzero fraction of the less-dense alloying components will fractionate into the inner core as it solidifies. Jephcoat and Olson (1987) extrapolated the density of pure iron to inner-core conditions and found that it is too dense to explain the inner-core seismic data, suggesting the inner core also contains some light alloy, equivalent to 3–7% sulfur by mass. Similarly, Laio *et al.* (2000) has calculated that solid iron under the conditions at the inner–outer core boundary is 2–3% more dense than given by PREM (Dziewonski and Anderson, 1981), and Lin *et al.* (2005) confirmed this experimentally by studying the sound velocities of pure iron at high pressure and temperature. Stixrude *et al.* (1997) calculated that the mass fraction of the less-dense element depends on which less-dense element and compound is present (for instance, FeS vs FeS_2). However, all estimates indicate the density jump at the inner–outer core boundary exceeds the $200\,kg\,m^{-3}$ expected for the phase transition alone, implying that light elements are segregating into the outer core.

Geochemists have examined the question of radioactive isotopes in the core, particularly U^{238}, Th^{232}, and K^{40}. Although the presence of radioactive heat had long been proposed as a source of energy for the geodynamo (Bullard, 1950; Gubbins *et al.*, 1979), the presence of heat-producing isotopes has long been questioned, as there is little experimental evidence for their solubility in liquid iron under core conditions (McDonough, 2003). Paleomagnetic evidence suggests that the Earth's magnetic field is at least 3 billion years old (McElhinny and Senanayake, 1980). Since the compositional buoyancy provided by inner-core solidification helps drive the dynamo (*see* Chapter 8.02), the inner core may be as old as the dynamo. However, thermal calculations (Labrosse *et al.*, 2001) suggest that such an old inner core is incompatible with the rate at which the inner core is currently growing. A resolution to this problem may be the presence of K^{40} in the core (Gessmann and Wood, 2002; Murthy *et al.*, 2003), which, with a half-life of 1.25 billion years, would have been an important heat source earlier in the Earth's history, allowing a slow rate of inner-core growth. Another possibility is that the power requirements of the dynamo are less than previously thought (Christensen and Tilgner, 2004), mitigating the need for an old inner core and hence radioactive heat sources. In light of all these uncertain possibilities the presence of radioactive elements in the core, and the age of the inner core, remain open questions.

8.10.2.2 Phase Diagram of Iron Alloy

Considerable work has been done in determining the alloy phase diagram of the core and the crystal structure of iron under inner-core pressure and temperature conditions. In a binary system with end members A and B, where each pure solid exists only in a single solid phase (crystal structure), and where A and B are miscible in the liquid phase, as is likely in the outer core (Alfe *et al.*, 1999; Helffrich and Kaneshima, 2004), three types of phase diagrams are possible. Which type of phase diagram exists for a given system is determined by the minimum in Gibbs free energy

$$G = H - TS \qquad [1]$$

where H is the enthalpy, T is the temperature, and S is the entropy. If the crystal structures are the same, and the atomic sizes are similar, then A and B may be completely miscible in the solid state as well as the

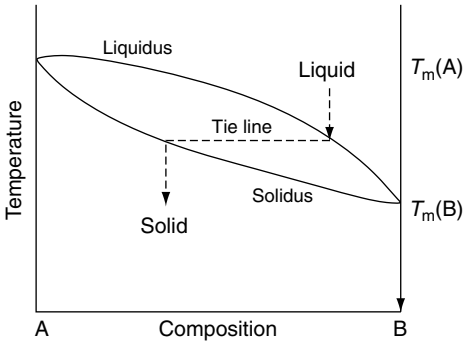

Figure 1 Phase diagram for a binary system (A,B) exhibiting complete solubility in both the liquid and solid phases (the enthalpy of mixing, ΔH, equals zero), so that both the liquid and solid phases are ideal solutions. The liquidus represents the temperature at which liquid of a given composition solidifies. A horizontal tie line at that temperature connects to the solidus, which gives the composition of the solid. The space between the curves represents the width of the phase loop, which is a measure of the compositional difference between the liquid and solid.

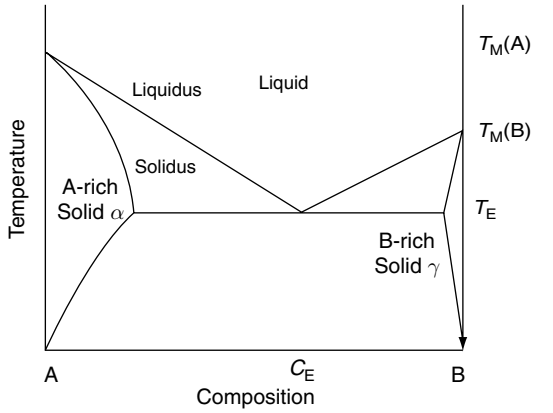

Figure 2 Phase diagram for a binary system exhibiting complete solubility in the liquid phase, but where $\Delta H > 0$ in the solids, so that the solids are real solutions. Because $\Delta H > 0$ in the solids, the system remains liquid to lower temperatures than the melting temperature of pure A or pure B (T_M(A) or T_M(B)). ΔH is sufficiently positive that the miscibility gap in the solid phase extends up to the liquid phase. Such a phase diagram represents a eutectic system. Two solid phases, A-rich α and B-rich γ, exist at all temperatures beneath the eutectic temperature T_E, the lowest temperature at which liquid can be in equilibrium with solid. At T_E, the composition of the liquid is C_E.

liquid state ($\Delta H = 0$ upon mixing). Liquid and solid are then both ideal solutions, and only two phases, liquid and solid, are possible in the temperature-composition field (**Figure 1**).

If the change in enthalpy upon mixing in the solid state is non-zero, then the solid is a real solution. If $\Delta H > 0$, atoms A and B are incommensurate, either because of a differing crystal structure, atomic size, or both. In this case it is energetically favorable for the mixture to remain a liquid to a temperature below that of the pure solid melting temperatures. Accompanying the melting point depression is a miscibility gap in the solid at low temperatures such that two solid phases co-exist. If ΔH is large enough, the miscibility gap can extend up to the liquid phase (Porter and Easterling, 1992). In this situation, the lower entropy associated with two separate solid phases, an A-rich α-phase and a B-rich β-phase (rather than randomly mixed atoms in a single phase), is made up for by the lower enthalpy that results from A and B existing primarily in separate phases.

Such a system exhibits a eutectic phase diagram (**Figure 2**), and there exists a eutectic composition that has a minimum melting temperature. Due to the entropic contribution, B will have nonzero solubility in the A-rich α-phase, and vice versa, but such a solid solution is not ideal. Examples of this type of phase behavior are ubiquitous, including model laboratory systems sodium chloride–water, ammonium chloride–water, lead–tin, and zinc–tin.

In a binary system with $\Delta H > 0$ it is also possible for stable solid phases other than those of pure A and pure B to exist. When such intermediate phases are present (as is common with iron alloys), a more complex phase diagram results. Other solidification reactions such as peritectic solidification can result. However, the essential solidification structure of the alloy is similar to that of a eutectic system (Porter and Easterling, 1992).

If $\Delta H < 0$, it is energetically favorable for a solid phase to form, so that a maximum in the melting temperature occurs for some intermediate composition. Such a solid is known as an ordered alloy because the atoms arrange themselves in a particular structure known as a superlattice. Ordered alloys often occur only within a certain compositional range. There is no experimental evidence that any of the possible core alloy components form an ordered alloy with iron under inner-core conditions.

At low pressures Fe–FeS forms a eutectic with a melting point depression of 600 K from that of iron. However, Boehler (1996a) has presented evidence showing that the melting point depression decreases with increasing pressure, based on experiments reaching pressures up to 62 GPa, still much lower than the 330 GPa at the inner–outer core boundary.

This suggests that Fe–FeS may form an ideal solid solution at inner-core pressures. This does not preclude an iron-enriched inner core, provided the liquidus and solidus are sufficiently separated in composition (the phase loop in **Figure 1** is wide), and the melting temperature of iron is higher than that of FeS, at core pressures. The latter may well be the case (Boehler, 1992; Anderson and Ahrens, 1996). However, Alfe *et al.* (2000) found from *ab initio* calculations that the concentration of sulfur in the solid state is very nearly that of the liquid state. Such a similarity in composition would seem to have difficulty explaining the excess density jump at the inner–outer core boundary. (The similarity indicates that the liquidus and solidus are close in composition. While this suggests an ideal solid solution, a eutectic system could still be a possibility if a significant fraction of the inner core has not yet cooled to the eutectic temperature (Fearn *et al.*, 1981).)

On the other hand, FeO alone may not be able to explain the presence of a less-dense component in the inner core. Sherman (1995), also using first-principles calculations, showed that the concentration of oxygen in the solid state is very low at inner-core pressures. However, Alfe *et al.* (1999) suggested that the concentration could be higher for other assumed crystal structures, and Stixrude *et al.* (1997) were able to explain the inner-core density with FeO present in solid solution with pure iron rather than as a mixture of separate phases.

Since the composition of the core remains uncertain, the phase diagram is also uncertain, but in spite of these uncertainties it is likely that a binary phase diagram captures the salient features of core solidification.

8.10.2.3 Crystal Structure of Iron

Understanding the solid phase(s) of pure and alloyed iron under inner-core conditions is central to interpreting the seismic anisotropy of the inner core (see Section 8.10.5). **Figure 3** summarizes the phase boundaries of iron. Under atmospheric pressure and room temperature, pure iron takes on a body-centered cubic (b.c.c.) crystal structure (the α-phase). At higher temperatures it undergoes a phase transformation to a face-centered cubic (f.c.c.) crystal structure (the γ-phase), and before melting it undergoes an entropy-driven phase transformation to another b.c.c. crystal structure (the δ-phase). At high pressure, pure iron transforms to a phase with a higher packing density, the hcp ε-phase. It has generally been

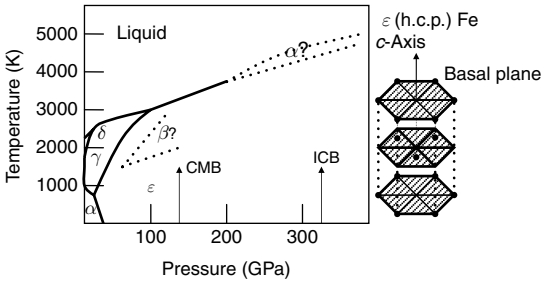

Figure 3 Summary of the phase boundaries of iron. The uncertainty of the boundaries increases with temperature and pressure, and the existence of the double h.c.p. β and b.c.c. α' phases is uncertain. To the right is the crystal structure of the h.c.p. ε phase.

thought that this is the stable phase of iron under inner-core conditions, though there have been some reports of a double h.c.p. phase (the β-phase; Saxena *et al.*, 1993). However, this experimental inference has been questioned (Vocadlo *et al.*, 1999; Kubo *et al.*, 2003). It has also been suggested that at the high temperatures of the inner-core, ε-iron could transform to a b.c.c. phase (Ross *et al.*, 1990; Matsui and Anderson, 1997; Belonoshko *et al.*, 2003). The role of impurities on the stable phases of iron under inner-core conditions is also under scrutiny (Vocadlo *et al.*, 2003).

8.10.3 Solidification of the Inner Core

Although hottest at the center, the inner core is solidifying directionally outwards due to the effect of pressure on the liquidus slope. A flat solid–fluid interface can become morphologically unstable (Mullins and Sekerka, 1963, 1964) due to constitutional supercooling (Rutter, 1958; Porter and Easterling, 1992). This occurs when rejection of solute during solidification of an alloy leads to a solute boundary layer in the fluid with a scale thickness D/V, where D is the solute diffusivity and V is the inner-core growth velocity. If the gradient of the local freezing temperature (the liquidus)

$$\mathrm{d}T_\mathrm{L}/\mathrm{d}z = \Delta T/(D/V) \qquad [2]$$

where ΔT is the temperature difference between the liquidus and solidus, exceeds the actual temperature gradient in the fluid, $\mathrm{d}T/\mathrm{d}z$, then freezing is predicted ahead of the flat solid–fluid interface (see **Figure 4**). This results in the growth of a solid perturbation into the fluid.

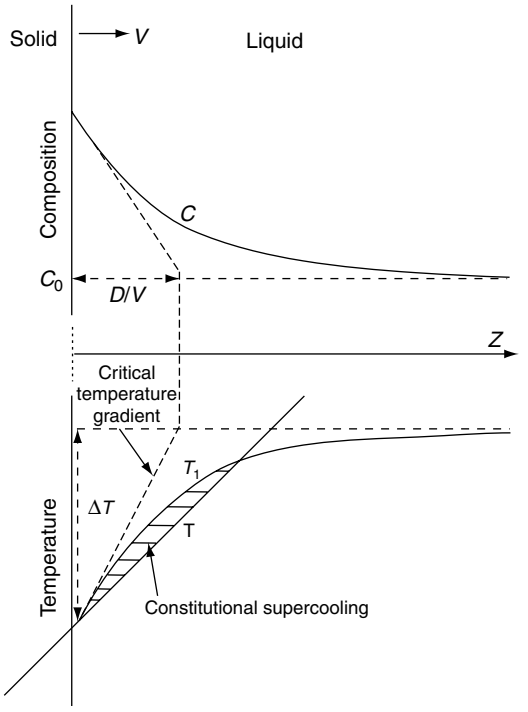

Figure 4 Dendritic growth in directionally solidifying alloys can occur when the liquid is constitutionally supercooled. Adjacent to the solid is a solute boundary layer of scale thickness D/V, where D is the solute diffusivity and V is the growth rate of the solid. The solute concentration C in the boundary layer is enriched relative to its value C_0 far from the solid. This enrichment depresses the equilibrium freezing temperature T_L by an amount ΔT from its value far from the solid. If the temperature T in the liquid is less than T_L, then solid is predicted ahead of the solid/liquid interface, a condition known as constitutional supercooling. The criterion for constitutional supercooling is that the temperature gradient in the liquid, $dT/dz < \Delta T/(D/V)$. Adapted from Porter DA and Easterling KE (1992) *Phase Transformations in Metals and Alloys*. London: Chapman and Hall.

Morphological instability due to constitutional supercooling typically results in dendritic growth of solute-poor solid, with interdendritic, solute-rich pockets. Dendrites oriented close to the direction of heat flow grow most rapidly (dendrites also grow in particular crystallographic directions, the key to solidification texturing). Directionally solidified alloys exhibit columnar crystals, elongated in the direction of dendritic growth (Porter and Easterling, 1992). The mushy zone is the mixed solid–fluid region during dendritic growth. Mushy zones are ubiquitous features in directionally solidifying metallic alloys, organic systems, and aqueous salt solutions on both sides of the eutectic, though they are less common in silicates because of the low entropy associated with faceted dendrites (Jackson, 1958; Miller and Chadwick, 1969).

Loper and Roberts (1981) extended the condition for morphological instability to include the effect of pressure variations on the liquidus, estimating that the inner-core growth rate is nearly 500 times supercritical. In essence, the argument for morphological instability of the inner-core boundary rests on the small temperature gradient dT/dz near the inner-core boundary, in spite of the inner-core growth velocity V also being very small. Fearn *et al.* (1981) suggested that the center of the Earth could exceed the eutectic temperature, so that the entire inner core would be in a mushy state.

Loper and Roberts (1978, 1980) also examined the thermodynamics of a slurry, which is a general mixed phase region. They considered an inner core formed by precipitation of heavy, iron-rich particles downwards. Shimizu *et al.* (2005) later considered the possibility that the inner core might in part grow by precipitation rather than dendritic growth, so that the region near the inner–outer core boundary might be a slurry layer rather than a mushy layer. They found, however, that morphological instability is likely for all realsitic values of the liquidus concentration slope.

Morse (1986, 2002) has questioned the prediction of a mushy inner core on other grounds – the assumption that heat and solute near the inner–outer core boundary are removed only by diffusion. Loper and Roberts (1981) ignored the effect of convection, arguing that it must become small near the boundary, but Morse (1986, 2002) suggests that convection at the base of the outer core reduces the solute buildup, making the inner-core growth rate nearly five orders of magnitude less than that needed for morphological instability.

Section 8.10.5.4 summarizes the seismic evidence for solidification structures in the inner core. There is also meteoritic evidence, although this evidence is ambiguous because of the relative lack of data and the large extrapolation from a meteorite to a planetary core. Iron meteorites such as those from the Cape York shower exhibit compositional gradients that are too large to result from the general fractionation of a planetoid core, but instead are more likely due to microsegregation between secondary and tertiary dendrite arms (Esbensen and Buchwald, 1982; Haack and Scott, 1992). Moreover, the FeS (troilite) nodules in meteorites are elongated and oriented, suggesting interdendritic pockets of melt during directional solidification (Esbensen and Buchwald, 1982).

8.10.4 Grain Size and Rheology in the Inner Core

The rheology of iron at core conditions governs the style and rate of deformation in the inner core. For timescales longer than the Maxwell relaxation time

$$\tau = \eta/G \quad [3]$$

the inner core can be considered to behave as a viscous fluid. Here η is the viscosity and G is the rigidity. Current estimates of inner-core viscosity span a large range, of the order 10^{13}–10^{21} Pa s, but even if the upper limit applies the inner core is less viscous than the mantle, because it is closer to its melting temperature. With a rigidity of the order of 10^{11} Pa (Dziewonski and Anderson, 1981), τ is between 10^2 and 10^{10}s, which is far shorter than mantle timescales. Constraints from rheology come from theoretical and empirical laws of mineral physics, and from elastic and anelastic properties of seismic waves at various frequencies. Here, we review the viscous properties followed by the elastic and anelastic properties.

Viscosity relates the stress σ to the strain rate $d\varepsilon/dt$. The general form of the strain rate in a solid can be expressed as

$$d\varepsilon/dt = A(DGb)/(kT)(b/d)^p(\sigma/G)^n \quad [4]$$

where D is the diffusion coefficient, b is the Burgers vector, k is Boltzmann's constant, T is temperature, d is the grain size, and p, n, and A are dimensionless constants (Van Orman, 2004).

Deformation occurs under imposed stress either by the diffusive movement of vacancies and atoms, or from slipping of lattice by dislocations (Poirier, 1985). Both of these mechanisms of deformation coexist, but the mechanism that gives the larger strain rate under a given stress becomes the predominant one. At high stress conditions, power law creep ($p = 0$, $n = 3$–5) gives the largest strain rate under a given stress. The nonlinear dependence of strain rate on stress results because the dislocation density increases with applied stress.

At low-stress conditions, both dislocation (Harper–Dorn creep) and diffusion creeps are possible. For large grain size, a Newtonian-type dislocation creep (Harper–Dorn creep, with $p = 0$, $n = 1$) dominates over diffusion creep. A Newtonian dependence is interpreted to arise from dislocation density that is independent of stress. One interpretation for the stress-independent dislocation creep was provided by Wang *et al.* (2002), who suggested that dislocation density results from the sum of two stresses: the applied stress and the Peierl's stress required to move the dislocations. For low-stress conditions Peierl's stress dominates, and the dislocation density becomes independent of applied stress. For small grain size, a Newtonian diffusion creep becomes faster. This is because the smaller grain size yields a larger spatial gradient of density of vacancies or atoms, which causes the deformation. There are two types of diffusion creeps: one where diffusion occurs within the lattice (Nabarro–Herring creep: $p = 2$, $n = 1$) and the other where diffusion occurs along the grain boundaries (Coble creep: $p = 3$, $n = 1$). The activation energy for grain boundary diffusion is smaller than that for lattice diffusion (Poirier, 1985), so for the high-temperature conditions of the inner core, Nabarro–Herring creep is more important.

These regimes of deformation are summarized in the form of deformation mechanism maps for various materials of interest (Frost and Ashby, 1982; also see **Table 1** for a general summary of the various high-temperature deformation mechanisms). Deformation mechanism maps are often constructed as a function of homologous temperature, T/T_m, (where T_m is the melting temperature) and normalized stress, σ/G. Compilation of data have shown that materials with the same crystal

Table 1 High temperature deformation mechanisms

	$p = 0$ (grain size independent)	$p = 2$	$p = 3$
$n = 1$(Newtonian)	Harper–Dorn creep (dislocation density independent of stress) Low stress Large grain size	Nabarro–Herring creep (diffusion within lattice) Low stress	Coble creep (diffusion along grain boundaries) Low stress Small grain size
$n = 3$–5	Power law creep (dislocation density increases with stress) High stress		

structure and similar bonding have similar deformation mechanism maps (Frost and Ashby, 1982), so h.c.p. metals can be used as an analog of h.c.p. iron to estimate the constants in eqn [4]. Homologous temperature of the inner core is high (>0.9), so we are left with estimating the magnitude of stress and grain size in order to estimate the viscosity of the inner core.

Several studies have sought to identify and quantify sources of stress in the inner core (see also Section 8.10.5). For instance, Jeanloz and Wenk (1988) considered a nonadiabatic large-scale degree-one flow in the inner core. They assumed a temperature variation of about 1 K with a length scale of 1000 km, and estimated that a buoyancy stress of about 10^4 Pa would arise. Together with the deformation mechanism of iron (Frost and Ashby, 1982), they estimated a viscosity of 10^{10}–10^{16} Pa s. This leads to a very large strain rate of the order of $10^{-9}\,s^{-1}$, or an equivalent flow velocity of about $10^{-3}\,m\,s^{-1}$, which is unrealistically fast.

Yoshida *et al.* (1996) considered an anisotropic inner-core growth and obtained a strain rate of the order of $10^{-18}\,s^{-1}$. Such a small strain rate is a result of a very slow growth rate of the inner core. They considered power law creep and Nabarro–Herring (diffusion) creep as possible candidates. From evaluating the stress needed to cause this strain rate, they showed that diffusion creep occurs for a grain size less than 6 m, and a power law creep occurs if the grain size is larger than 6 m, though there are uncertainties in the parameter values used. As an additional condition, they assumed that dynamic recrystallization governs the grain size, which yields a smaller grain size for larger stress. Using these constraints, they obtained a grain size of 5 m, which is marginally in the diffusion creep regime, and a viscosity of 3×10^{21} Pa s. In another model, they applied a Maxwell relaxation model to seismic attenuation data, and estimated the viscosity to be greater than 10^{16} Pa s.

Bergman (1998, 2003) examined the issue of grain size in the inner core. One constraint on grain size comes from assuming that the frequency-dependent inner core attenuation (see Section 8.10.5.4 of this chapter) arises from scattering (e.g., Cormier *et al.*, 1998; Cormier and Li, 2002). For this case, the grain size becomes large, of the order of a seismic body wavelength, that is, 100 m to 1 km (Bergman, 1998). It is also possible to estimate the grain size from extrapolation of dendrite size obtained from laboratory experiments (although by six orders of magnitude!). Due to the slow cooling rate in the inner core, the grain size estimate is of the order of a few hundred meters (Bergman, 2003).

Van Orman (2004) argued that Harper–Dorn creep is the dominant deformation mechanism in the inner core. This mechanism occurs at low stress and large grain size conditions, a regime not considered by Yoshida *et al.* (1996). For the low stress level in the inner core, Van Orman (2004) showed that power law creep is unlikely, and that Harper–Dorn creep would occur for grain sizes exceeding 10–30 μm. In this likely case, the estimated viscosity becomes 10^{10}–10^{12} Pa s, which is quite small. The deformation mechanism in the inner core thus remains unclear.

It is important to note that the above estimates are for solid h.c.p. iron. The presence of melt within the inner core would drastically reduce the viscosity, so that the above estimates should be taken as an upper limit. In addition, the presence of melt would promote diffusion of atoms along grain boundaries, and cause pressure solution-type creep (which is similar to Coble creep), thus resulting in a grain-size dependence.

8.10.5 Origin of the Inner-Core Elastic Anisotropy

8.10.5.1 An Overview

Inner-core elastic anisotropy, where P-waves travel about 3% faster in the polar direction than parallel to the equatorial plane, with a larger degree of anisotropy in the deeper inner core, is well established from seismic body waves and free oscillations. The most plausible interpretation, based on the analogy with mantle anisotropy, is that it results from the lattice-preferred orientation of the h.c.p. iron that comprise the inner core. Alternatively, it could be due to shape-preferred orientation of melt pockets (Singh *et al.*, 2000). Seismology has also shown that there is an attenuation anisotropy, where P-waves in the polar direction are more attenuated (see Section 8.10.5.4; Creager, 1992; Song and Helmberger, 1993; Souriau and Romanowicz, 1996, 1997; Yu and Wen, 2006).

A variety of models have been proposed to explain the origin of inner-core elastic anisotropy. We can classify them into two categories. The first category consists of dynamical models, which assume the crystals align as a result of plastic deformation within the inner core. The second set of models assume that the inner-core texture forms during solidification from the liquid outer core. **Table 2** lists the advantages and drawbacks of each of the models. In the next subsection we summarize the anisotropic properties of h.c.p. iron and its style of slip under dislocation creep, followed by a

Table 2 Models for inner-core anisotropy

Mechanism	Reference	Advantages	Drawbacks
Deformation models			
Inner-core thermal convection	Jeanloz and Wenk (1988)	Analogy with mantle	Inner core not likely to be thermally convecting
Preferential equatorial solidification due to outer core convection	Yoshida, *et al*. (1996)	Explains relation of fast axis with spin axis, preferential solidification observed in lab experiments	Low stress levels so that texture may take age of IC to develop
Radial component of Maxwell stress	Karato (1999)	Anisotropy reflects magnetic field, larger stress level	Stress likely to be balanced by other stresses
Azimuthal component of Maxwell stress	Buffett and Wenk (2001)	Can sustain flow	Requires *c*-axis to be slow, depth dependence?
Solidification models			
Paramagnetic susceptibility	Karato (1993)	Novel	Iron under inner-core conditions not likely to be paramagnetic
Anisotropic heat flow due to outer core convection	Bergman (1997)	Observed in lab, simple depth dependence, may also explain attenuation anisotropy	Requires *c*-axis to be fast, effects of deformation?

None of the models by themselves can easily explain latitudinal variations, or abrupt changes with depth.

review of the two categories of models for understanding inner-core elastic anisotropy.

8.10.5.2 Anisotropy of h.c.p. Iron

The anisotropy of h.c.p. iron at inner-core conditions was first estimated from analog h.c.p. metals. Wenk *et al.* (1988) considered Ti at room conditions to be a good analog for the inner core because it has a similar c/a ratio and ratio of linear compressibility as h.c.p. iron. They concluded that P-waves should be faster in the *c*-axis direction. Sayers (1989) analyzed several h.c.p. metals and arrived at the same conclusion. These estimates were based on room temperature values. Bergman (1998) argued, based on the temperature dependence of the elastic constants of h.c.p. metals, that the magnitude of anisotropy of h.c.p. iron would become even larger at core temperatures.

In recent years, first-principles calculations and high-pressure experiments have made direct determination of elastic constants possible (Steinle-Neumann *et al.*, 2003). Stixrude and Cohen (1995) calculated elastic constants of h.c.p. iron at core pressures (but 0 K), again finding the *c*-axis fast, by about 4% for compressional waves. These calculations were then extended to high temperatures by Steinle-Neumann *et al.* (2001), who found that the sense of P-wave anisotropy reversed from that at 0 K, so that the *a*-axis of a single crystal is 10–12% faster than the *c*-axis at high temperature. According to Steinle-Neumann *et al.* (2001), the seismic inference of a 3% fast P-wave velocity in the polar direction can thus be explained by 1/3 alignment of *a*-axes (or basal planes) in the polar direction. However, calculations by Gannarelli *et al.* (2003) did not find a reversal of the sense of anisotropy. Experimental determination of the elastic constants by Mao *et al.* (1998, 1999) inferred a bulk modulus and rigidity similar to previous values, but with the fast axis lying at an angle intermediate between the *c*- and *a*-axes.

If the preferred orientation of h.c.p. iron occurs by dislocation creep, a critical issue is whether the predominant slip plane is basal or prismatic. Poirier and Price (1999) applied the criterion derived by Legrand (1984) to determine whether basal or prismatic slip dominates in h.c.p. iron. To distinguish between the various slip regimes, Legrand (1984) defined a parameter R as

$$R = (c_{66} \cdot \gamma_B)/(c_{44} \cdot \gamma_P) \qquad [5]$$

where c_{66} and c_{44} are elastic constants and γ_B and γ_P are the stacking fault energies in the basal and prism planes, respectively. Legrand (1984) showed that when $R < 1$ the primary slip system is basal and when $R > 1$ it is prismatic. Using *ab initio* calculations, Poirier and Price (1999) calculated the stacking fault energies for h.c.p. iron, and using the published elastic constants for 0 K h.c.p. iron, they found that R becomes 0.37–0.43, indicating that h.c.p. iron slips predominantly on the basal

plane. This result is also obtained when the elastic constants of Steinle-Neumann *et al.* (2001) are used.

Wenk *et al.* (2000b) conducted high-pressure deformation experiments of h.c.p. iron in a diamond anvil, at pressures of up to 220 GPa. By imposing a uniaxial nonhydrostatic stress, they found that *c*-axes align parallel to the axis of the diamond cell. Comparing with the results from plasticity theory, they found that basal slip is dominant in determining the overall preferred orientation even if prismatic slip is favored over basal slip.

8.10.5.3 Dynamical Models

The key issues for a dynamical origin of the preferred orientation are the source and pattern of stress, and the mechanism of alignment. The first of the dynamical models was by Jeanloz and Wenk (1988), who proposed that preferred orientation of h.c.p. iron is caused by inner-core convection driven by internal heat sources. By evaluating the radiogenic heat generation in the inner core, they concluded that the Rayleigh number in the inner core is supercritical. They showed that if a spherical harmonic degree $l = 1$ convection exists in the inner core, then the resulting simple shear flow in the equatorial region yields a *c*-axis alignment of about 45° from the polar direction. Averaging such a crystal alignment, and using the elastic constants of Ti, Jeanloz and Wenk obtained a fast P-wave in the polar direction. There are, however, several issues with this model. First, the amount of radiogenic heat is highly uncertain so that thermal convection in the inner core may not occur. Thermal history calculations generally do not yield thermal convection in the inner core because the geothermal gradient in the inner core becomes smaller than the adiabat (due to the slow growth rate of the inner core), which allows sufficient time for the inner core to cool (Sumita *et al.*, 1995; Yoshida *et al.*, 1996; Yukutake, 1998). Also, this model does not explain why a degree 1 convection pattern with a symmetry axis corresponding to the rotation axis should be preferred. Later, numerical studies of thermal convection in the inner core were carried out by Weber and Machetel (1992), and by Wenk *et al.* (2000a). In the latter study, preferred orientation of h.c.p. iron under a polar downwelling and an equatorial upwelling was calculated, which resulted in a fast P-wave in the polar direction.

An explanation for an inner-core flow pattern with an axis coinciding with the rotation axis was given by Yoshida *et al.* (1996). They argued that the inner-core growth should be of zonal degree 2 because of the columnar convection in the outer core, which transports heat more efficiently from low latitudes of the inner core. This causes the inner core to grow faster near the equator (see **Figure 5**). Experiments conducted by

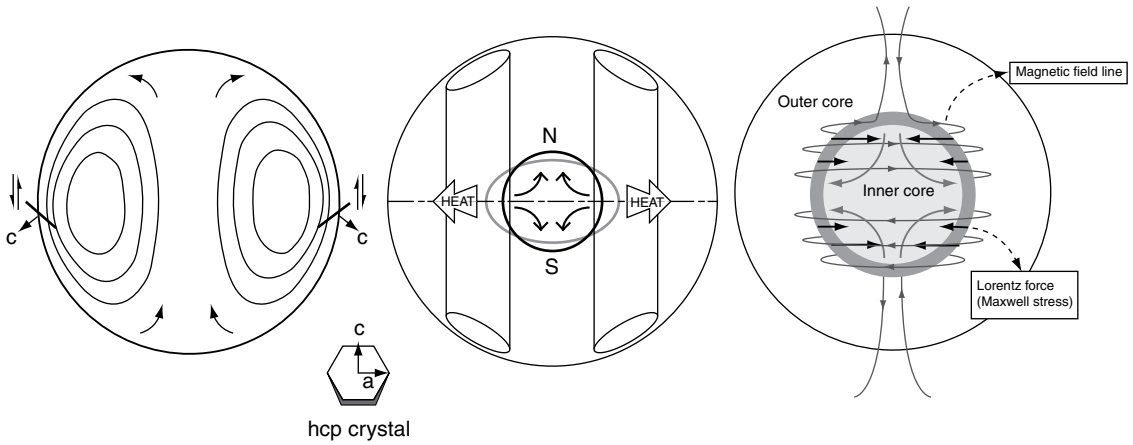

Figure 5 Some dynamical models exhibiting a radial flow in the inner core. In these models such flow is considered to be responsible for the preferred orientation of crystals. (a) An internally heated inner core can convect. A degree 1 mode is the first unstable mode. Adapted from Jeanloz R (1990) The nature of the Earth's core. *Annual Review of Earth and Planetary Sciences* 18: 357–386. (b) Convection in a rapidly rotating, spherical fluid shell such as the outer core is more efficient at transporting heat perpendicular to the rotation axis. This leads to an inner core that solidifies more oblately than the gravitational equipotential. A solid-state flow results, and the stress may lead to a recrystallization texture. Adapted from Yoshida S, Sumita I, and Kumazawa M (1996) Growth model of the inner core coupled with outer core dynamics and the resulting elastic anisotropy. *Journal of Geophysical Research* 101: 28085–28103. (c) Maxwell stresses resulting from the magnetic field in the outer core can squeeze the inner core, causing a flow. Here a toroidal magnetic field is shown to cause such flow. In this model, the flow pattern depends on the magnetic field pattern of the outer core. Adapted from Karato S (1999) Seismic anisotropy of the Earth's inner core resulting from flow induced by Maxwell stresses. *Nature* 402: 871–873.

Bergman *et al.* (2005) show this effect in a rotating hemisphere of salt water solidifying from the center. However, because of the density difference between the inner and outer cores, the inner core must deform isostatically to maintain its spherical shape, and an overall stress field with uniaxial tension in the polar direction results. Using the elastic constants of Stixrude and Cohen (1995) and Kamb's theory of preferred orientation by recrystallization under stress (Kamb, 1959), Yoshida *et al.* (1996) showed that this model can explain the observed inner-core anisotropy. Sumita and Yoshida (2003) used the same model with the elastic constants of Steinle-Neumann *et al.* (2001) and found that *a*-axes aligning in the polar direction can explain the sense of anisotropy. One problem with this model is that the stress resulting from anisotropic growth is quite small due to the slow growth rate of the inner core. As a result, preferred orientation would take a geologically long time (on the order of 10^9 years) to develop. The applicability of Kamb's theory under the presence of dislocations is also uncertain.

Karato (1999) argued that Maxwell stresses resulting from the geomagnetic field generated in the outer core could also induce flow in the inner core, by radially squeezing the inner core at the ICB. In this model, a toroidal magnetic field of $B = 10^{-2} - 10^{-1}$ T results in Maxwell stresses $\sigma = 10^2 - 10^4$ Pa. Since the induced flow pattern in the inner core is controlled by the magnetic field pattern in the outer core, this model predicts that the inner-core anisotropy reflects the magnetic field pattern. However, Buffett and Bloxham (2000) questioned whether the Maxwell stresses can actually drive a radial flow in the inner core, or whether they are simply balanced by other stresses. They considered the balance between magnetic, pressure and buoyancy stresses, and showed that these stresses would not equilibrate because of the incompatibility between thermodynamic and hydrostatic equilibrium conditions at the ICB. As a result, they predict that viscous flow would occur, but they also showed this flow to be weak and confined near the ICB. As a result, they concluded that the radial component of the Maxwell stress is unsuitable for causing preferred orientation.

Buffett and Wenk (2001) used the elastic constants by Steinle-Neumann *et al.* (2001), and considered the Lorentz force tangential to the inner core. They calculated the resulting anisotropy that forms under an inner-core shear flow. The resulting stress in this model becomes quite small, of the order of several Pa. Assuming both basal and prismatic slips to occur for h.c.p. iron, they showed that the *c*-axes become parallel to the equatorial plane, which is consistent with the seismic inferences, if the *c*-axis of h.c.p. iron under inner-core conditions is indeed the slow direction. Since the Maxwell stress decreases with the distance from the inner-core boundary, the alignment becomes weak with depth, so that an explanation is needed to produce a stronger anisotropy with depth. Another issue is that the stress field depends strongly on the morphology of the magnetic field, which is not known well.

To summarize, the condition of thermodynamic equilibrium at the ICB is important in evaluating the flow pattern in the inner core, as the analysis of Buffett and Bloxham (2000) showed. Since the flow pattern in the outer core, the solidification at the ICB, and the pattern and magnitude of Maxwell stresses are all coupled, a self-consistent model of inner-core anisotropy needs to properly incorporate all of these effects.

8.10.5.4 Solidification Texturing Models

The second category of models to explain the origin of inner-core anisotropy invoke solidification. Karato (1993) proposed that h.c.p. iron may have a paramagnetic susceptibility and would align during solidification under a magnetic field, hence resulting in a preferred orientation. However, this model predicts larger anisotropy near the ICB, which is inconsistent with the observations. Furthermore, theoretical studies show h.c.p. iron to be nonmagnetic at core pressures (Söderlind *et al.*, 1996; Steinle-Neumann *et al.*, 1999).

A solidification texturing during directional cooling was shown by Bergman (1997) to be a possible mechanism for understanding inner-core elastic anisotropy. The directional cooling occurs perpendicular to the rotation axis, as a result of the pattern of convection in the outer core, as suggested by Yoshida *et al.* (1996), later demonstrated in experiments by Bergman *et al.* (2005). Solidification experiments on tin-rich alloys exhibit dendrites that grow in a particular crystallographic direction controlled by the direction of heat flow, resulting in elastic anisotropy. This result was extended to h.c.p. zinc alloys by Bergman *et al.* (2000). Hence, the direction of heat flow becomes a preferred crystallographic direction (**Figure 6**). The geometry of the crystal growth results in an increase in anisotropy with depth. The effect of fluid flow on solidification texturing of h.c.p. zinc alloys was examined by Bergman *et al.* (2003). In analogy with the solidification of h.c.p. sea ice, the experiments showed that the fluid flow causes

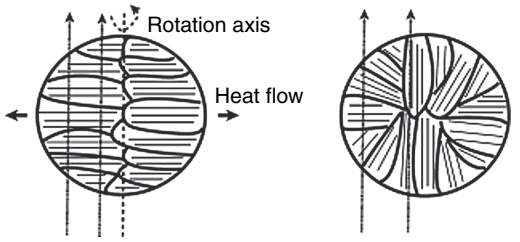

Figure 6 A solidification texturing model resulting in a preferred orientation of crystals. Heat flow perpendicular to the rotation axis leads to dendritic growth in the cylindrically radial direction. The heavier lines represent columnar crystals, the lighter lines primary dendrites. The left panel represents a longitudinal cross section, the right panel an equatorial cross section. North–south seismic rays (left panel), represented by the dotted arrows, are always perpendicular to the growth direction of dendrites. The component of rays perpendicular to the rotation axis (right panel) that is parallel to the growth direction of dendrites increases with turning depth in the inner core. This is the origin of the depth dependence associated with solidification texturing of the inner core. (Such geometric depth dependence becomes less strong for rays not turning on the equatorial plane.) Adapted from Bergman MI (1997) Measurements of elastic anisotropy due to solidification texturing and the implications for the Earth's inner core. *Nature* 389: 60–63.

transverse texturing, indicating that alignment is sensitive to the direction of fluid flow as well as that of heat flow.

Brito *et al.* (2002) conducted directional solidification experiments using liquid (pure) gallium, and measured the resulting anisotropy of the polycrystalline gallium. They found that for all cases crystals elongated parallel to the imposed thermal gradient that determined the direction of crystal growth, and that other factors such as turbulence and magnetic field have little influence. They also found that the preferred orientation of crystals is controlled primarily by the presence of seed grains, and that this strongly affects the amount of anisotropy. Seeding has been observed to have more of an effect on the texture of solidifying fresh water than salt water (Weeks and Wettlaufer, 1996). Unresolved issues with solidification texturing include whether conduction will dominate over convection as regards heat transport in the outer core, the role of post-solidification deformation in modifying the solidification texture, whether the observed depth dependence can be explained by the simple depth dependence predicted by geometry, and uncertainty as to the sense of fastest wave propagation in h.c.p. iron under inner-core conditions.

8.10.6 Origin of Other Inner-Core Seismic Structures

In this section we review other seismic structures of the inner core, and their geodynamical interpretations.

8.10.6.1 Properties and Structure of the Inner-Core Boundary

The inner-core boundary has been found to be seismically sharp, with a transition thickness of less than 5 km (Cummins and Johnson, 1988). Such a sharp inner-core boundary may be explained by a rapid increase in solid fraction of partial melt with depth, which might result from convection within the mushy layer (Loper, 1983) or from compaction (Sumita *et al.*, 1996). It has been proposed that the inner-core radius may depend on frequency, if the inner-core boundary is a diffuse boundary defined by the relaxation time equivalent to the period of a seismic wave (Anderson, 1983). However, this has not been substantiated, which indicates that the inner-core boundary is probably not a gradual transition from the outer core to the inner core.

We next consider structure near the inner-core boundary. At the high pressures of the Earth's core, the difference between the bulk modulus of the solid and liquid is small. As a result, the P-wave velocity jump at the inner-core boundary arises primarily from the finite rigidity of the inner core. The bottom most part of the outer core has been found to have a small to zero P-wave velocity gradient compared to PREM (Souriau and Poupinet, 1991; Song and Helmberger, 1992, 1995; Kaneshima *et al.*, 1994). One interpretation is that this is a layer with solid crystals that are not interconnected, such that the rigidity is zero. P-wave velocity in this layer is then given approximately by the Wood's formula (Mavko *et al.*, 1998)

$$V = (K_R/\rho)^{1/2} \qquad [6]$$

where K_R is the Reuss average of the bulk modulus of the solid–liquid composite, and ρ is the average density.

If we use the values at the top of the inner core for solid and bottom of the outer core for liquid, then we find that the average density increases more with solid fraction than does the average bulk modulus. As a consequence, P-wave decreases with solid fraction. For example, a 20% volumetric fraction of solid particles yields a velocity decrease of approximately

0.2%. Highly porous dendrites such as those observed in the solidification of ammonium chloride crystals, which does not allow shear waves to propagate, may be analogous to such a layer. Such a layer also results in attenuation. A frequency-dependent attenuation at the top of the outer core has been reported (e.g., Tanaka and Hamaguchi, 1993). A similar analysis for the bottom of the outer core may be used to constrain the solid fraction in this layer (Stevenson, 1983). An apparent absence of scattering in this layer, may also be used to constrain the length scale of dendrites.

8.10.6.2 Inner-Core Attenuation and Scattering

Knowledge of seismic attenuation in the inner core could give earth scientists considerable insight into the nature of the inner core, but at present the depth and frequency dependence of the seismic quality factor in compression Q_α or in shear Q_β remain uncertain (Masters and Shearer, 1990). At body-wave frequencies (1 Hz), Q_α in the upper inner core is quite low, about 200, increasing to 440–1000 deeper into the inner core (Cormier, 1981; Doombos, 1983; Souriau and Roudil, 1995). Using normal modes, Widmer *et al.* (1991) found Q_β to be even lower, about 120. Little depth resolution is available from normal-mode data.

Taken together these studies could indicate a frequency dependence of attenuation, or high attenuation in compression, but mineral physicists are not in agreement. Mao *et al.* (1998) found that the aggregate shear wave speed of h.c.p. iron extrapolated from 220 GPa and room temperature to inner-core conditions is about 15% greater than that in the inner core (Dziewonski and Anderson, 1981), suggesting near-melting softening. However, some studies (Jackson *et al.*, 2000; Laio *et al.*, 2000; Steinle-Neumann *et al.*, 2001) found a Poisson's ratio for h.c.p. iron under inner-core conditions comparable to that from PREM, suggesting that the high Poisson's ratio of the inner core is an intrinsic property of h.c.p. iron at high temperature.

Attenuation in the inner core can result from intrinsic relaxation and diffusion mechanisms, and from scattering. As seismic waves travel they cause an adiabatic pressure perturbation, which causes a temperature change and, potentially, freezing and melting. These cause thermal and compositional diffusion, and result in attenuation. Loper and Fearn (1983) derived an expression for frequency-dependent attenuation due to diffusion. Under this mechanism, attenuation increases with melt fraction, with peak attenuation at the timescale corresponding to thermal and compositional diffusion.

Singh *et al.* (2000) evaluated the attenuation for the case where liquid can flow in the interconnected space of a solid matrix, as a result of the pressure variations arising from the propagation of seismic waves. In the seismic frequency range of interest, their results showed an attenuation peak at a viscosity of around 250 Pa s. Likely values for the molecular viscosity of iron at core conditions (Section 8.10.4) are five orders of magnitude smaller than this, so that attenuation from this mechanism is negligibly small.

Another interesting finding is the coda waves following the inner-core-reflected wave (PKiKP) (e.g., Vidale and Earle, 2000). One interpretation is that these are caused by strong scatterers with a scale length of about 2 km in the outermost 300 km of the inner core (Vidale and Earle, 2000). They may alternatively be due to reverberation effects near the inner-core boundary (Poupinet and Kennett, 2004). Laboratory experiments indicate that there are at least three length scales associated with solidification that could be relevant to scattering: the grain size, the spacing between dendrites, and the spacing between the chimneys of the upwelling in the mushy layer (e.g., Tait *et al.*, 1992). Reverberation near the inner-core boundary might be caused by waves trapped in a low-Q mushy zone between the high-Q outer core and the deeper inner core.

Scattering can give rise to an apparent Q that is lower than the intrinsic material value. This has been explored by Cormier (1981) and Cormier and Li (2002) for 10–30 km wavelength body waves. Bergman (1998) and Cormier *et al.* (1998) also examined whether anisotropic scattering as a result of columnar crystal growth might also be responsible for an attenuation anisotropy (Creager, 1992; Souriau and Romanowicz, 1996, 1997; Oreshin and Vinnik, 2004; Yu and Wen, 2006), where waves traveling parallel to the fast rotation axis exhibit smaller amplitudes and more complex waveforms. Anisotropic scattering has been observed in directionally solidified h.c.p. zinc alloys (Bergman *et al.*, 2000). Like the elastic anisotropy, the attenuation anisotropy may also have a hemispherical variation. On the other hand, some studies have shown that there are regions without such attenuation anisotropy (Helffrich *et al.*, 2002).

8.10.6.3 Hemispherical Variation of Seismic Velocity, Anisotropy, and Attenuation

Next we turn to laterally heterogeneous structures in the inner core. Recent seismological studies have revealed that there exists a large-scale longitudinal variation in P-wave velocity and its anisotropy, which appears to be depth dependent. Using P-waves traveling in the east–west direction, it was found that the eastern hemisphere has a larger Vp and also a smaller Q compared to the western hemisphere (Tanaka and Hamaguchi, 1997; Niu and Wen, 2001; Wen and Niu, 2002; Cao and Romanowicz, 2004), and using P-waves traveling in the polar direction, it was found that the Western Hemisphere has a larger anisotropy compared to the Eastern Hemisphere (e.g., Tanaka and Hamaguchi, 1997; Creager, 1999). Furthermore, Cao and Romanowicz (2004) found a hemispherical variation of the depth dependence of attenuation of P-waves. Their results indicate that Q in the Eastern Hemisphere increases with depth, whereas that in the Western Hemisphere decreases with depth. Since the outer core and deep inner core have a large Q, a minimum Q should exist somewhere near the ICB. They proposed that this minimum exists at a deeper depth in the Western Hemisphere compared to the Eastern Hemisphere.

Such hemispherical structure may be produced by lateral variation of the inner-core solidification rate, caused by the outer-core flow controlled by the thermally heterogeneous mantle (Sumita and Olson, 1999, 2002). More rapid solidification of the inner core in the Western Hemisphere would lead to a porous inner core because there is insufficient time to expel liquid by compaction, leading to a low Vp there. Similarly, if the inner-core anisotropy results from preferential growth, the Western Hemisphere would have a larger anisotropy. On the other hand, long-term mantle control to explain hemispherical variations requires that the inner core be locked to the mantle (Buffett, 1996b), implying that seismologists are inferring an inner-core oscillation rather than a rotation. Future observations should resolve this issue. There may also be some positive feedback mechanism, for example, involving an anisotropic thermal conductivity, but this has not yet been studied in detail.

We also need to consider the origin of the hemispherical difference of the depth of minimum Q proposed by Cao and Romanowicz (2004). There are at least two candidates for the laterally variable minimum Q that arise from the variation of melt fraction. One results at a very low melt fraction at a temperature just above the eutectic. This is inferred from the acoustic measurements of a partially molten binary eutectic system (e.g., Spetzler and Anderson, 1968; Stocker and Gordon, 1975; Watanabe and Kurita, 1994). These experiments have shown that as the temperature is raised, Q abruptly decreases at the eutectic temperature, but recovers slightly at higher temperatures, before decreasing at yet higher temperatures. Another candidate for a minimum Q exists at a much higher melt fraction, since the liquid outer core has a high Q. However, these two candidates have caveats. If the cause of the minimum is a very low melt fraction, then there should be a stepwise increase of Q at a certain depth corresponding to the eutectic temperature. However, this has not yet been observed. On the other hand, if the minimum occurs at a higher melt fraction, then the melt fraction cannot be too high so as to inhibit shear wave propagation. It is uncertain whether such melt fraction can be realized within the inner core.

8.10.6.4 The Deep Inner Core and the Inner-Core Transition Zone

Finally, we consider the seismic structure of the deeper section of the inner core. Deeper in the inner core attenuation has been found to be smaller, which may be explained by a smaller liquid fraction or from a larger grain size. Seismic anisotropy is found to be larger in the deeper inner core (e.g., Creager, 2000), with a possible transition zone at about 200 km depth between the isotropic and anisotropic inner core (Song and Helmberger, 1998), and laterally variable. However, the sharpness of this transition seem to differ for different wavelengths and geographical locations (Leyton *et al.*, 2005).

Several possible explanations can be given for the cause of larger anisotropy with depth. A smaller anisotropy at shallow parts can arise from random alignment in the horizontal plane or from alignment such that the symmetry axis (c-axis for h.c.p.) is in the radial direction. The former can result from the slow kinetics of crystal alignment, the geometry of solidification texturing, or fluid flow in the outer core, and the latter from a principal stress axis in the radial direction at shallow depths. Such a stress field may arise from electromagnetic stresses or from compaction. Some observations even suggest that the deepest part of the inner core may be

distinctly different from other parts of the inner core (Ishii and Dziewonski, 2002, 2003; Beghein and Trampert, 2003), perhaps suggesting a phase transition from h.c.p. to b.c.c. iron.

8.10.7 Inner-Core Rotation

8.10.7.1 An Overview

Inner-core rotation relative to the mantle was first proposed on theoretical grounds by Gubbins (1981), and then found to occur, on the order of degrees per year, in numerical dynamo models by Glatzmaier and Roberts (1995a, 1995b). Following the numerical simulations, Song and Richards (1996) inferred that the tilted symmetry axis of inner-core anisotropy is rotating eastward about the spin axis, at a rate of 1.1 deg yr^{-1}, and Su *et al.* (1996) found a rate as high as 3 deg yr^{-1}. However, using a lateral anisotropy gradient rather than the tilted symmetry axis, Creager (1997) limited the differential rotation to 0.2–0.3 deg yr^{-1}. In these studies there is a tradeoff between the rate of super-rotation and the level of anisotropy and symmetry axis tilt, or the anisotropy gradient. Vidale *et al.* (2000) examined the PKiKP coda from nuclear tests, which eliminates tradeoffs associated with event mislocations, to also infer a differential rotation rate of 0.2 deg yr^{-1}. However, using the splitting of core-sensitive normal modes, Laske and Masters (1999) preferred no rotation, though the data allows a maximum inner-core super-rotation of 0.2–0.3 degrees yr^{-1}. Numerical simulations with a better resolution and less hyper-diffusion also predict a modest prograde inner-core rotation of about 0.1 degrees yr^{-1}, which further decreases to 0.02 degree yr^{-1} when gravitational coupling is included (Buffett and Glatzmaier, 2000). Although there have been controversial seismological issues (Souriau and Poupinet, 2003), recent studies using earthquakes with similar waveforms (Zhang *et al.*, 2005) continue to support inner-core super-rotation. Here we review mechanisms that can cause as well as inhibit inner-core rotation.

8.10.7.2 Electromagnetic Coupling

Various torques can act on the inner core and these can make the inner core rotate. Electromagnetic torque was considered by Gubbins (1981) and was also the driving mechanism in the numerical models by Glatzmaier and Roberts (1995a, 1995b). Electromagnetic torque originates from the restoring force caused by the outer-core flow that stretches the magnetic field lines. It is expressed as (Rochester, 1962)

$$\Gamma = 1/\mu_0 \int (B_r B_\phi \, r \sin\theta \, \mathrm{d}S) \qquad [7]$$

where μ_0 is the magnetic permeability, B_r and B_ϕ are the radial and azimuthal fields at the ICB. Quantitative estimates of inner-core rotation from electromagnetic torque were given by Gubbins (1981). He showed that when an electromagnetic torque of 10^{19} Nm is applied to the inner core, it would rotate and approach a steady angular velocity of about 0.13 deg yr^{-1}, and induce a toroidal magnetic field of about 80 gauss. He also showed that an oscillatory motion with a period of about 10 years is possible.

The mechanism of inner-core rotation in the numerical calculations by Glatzmaier and Roberts (1995a, 1995b) was analyzed in Glatzmaier and Roberts (1996). They showed that the electromagnetic coupling caused by the thermal wind within the inner-core tangent cylinder was the primary cause. Within the tangent cylinder, upwellings form above the polar region and downwellings near the equator. This meridional circulation causes eastward flow near the inner core and westward flow near the core–mantle boundary, by conservation of angular momentum. The eastward flow, coupled with the magnetic field, results in an electromagnetic coupling between the outer-core flow and the inner core, and spins up the inner core.

An analytical model of inner-core rotation driven by the thermal wind was also derived by Aurnou *et al.* (1996). Assuming that the temperature inside the tangential cylinder is higher than the temperature outside, they showed that the resulting eastward thermal wind, coupled with the magnetic field, can quantitatively explain the inner-core superrotation. This model was extended in Aurnou *et al.* (1998) by numerically calculating the resulting inner-core rotation from electromagnetic coupling for three different outer-core flow patterns. This work confirmed that the thermal wind can efficiently couple inner-core rotation to outer-core flow.

8.10.7.3 Gravitational Coupling

Mass anomalies in the mantle can deform the inner core. When the inner core rotates relative to the mantle, a misalignment of the inner core topography relative to the mantle mass anomaly causes a gravitational restoring force to the inner core.

This torque was shown to become quite large, of the order of 10^{21} N m by Buffett (1996b). Although there are uncertainties in the mass anomaly within the mantle, this estimate indicates that a gravitational torque can exceed the electromagnetic torque by orders of magnitude, and thus lock the inner core to the mantle to inhibit rotation. Such gravitational coupling between the mantle and the inner core can cause an exchange of angular momentum between them, and result in length-of-day variations (Buffett, 1996a, 1996b).

Gravitational torque can become small if the inner-core topography cannot become as high as that caused by the mass anomaly of the mantle. If this torque becomes smaller than the electromagnetic torque, the inner core may rotate. Buffett (1997) showed that it is possible to constrain the viscosity of the inner core if the inner core is rotating under the gravitational torque. One case is when the viscosity of the inner core is so small that the inner core can deform rapidly, and thus misalignment of the mantle mass anomaly and inner-core topography does not occur. The other case is when the viscosity of the inner core is so high that the inner core is slow to deform and thus the inner-core topography becomes small. For this case, however, because of high viscosity, once it becomes locked to the mantle, it would become unable to rotate again. From the above constraints, the inner-core viscosity was found to become less than 10^{16} Pa s or greater than 10^{20} Pa s.

8.10.7.4 Combined Coupling

Estimates of electromagnetic torque have large uncertainty because the strength of the toroidal field inside the core cannot be observed. Aurnou and Olson (2000) calculated the inner-core rotation under the combined effects of electromagnetic, gravitational, and viscous torques. Among these torques, the viscous torques was found to be very small. When the electromagnetic and gravitational torques are comparable, the inner-core rotation showed time-dependent features. A more general case of inner-core rotation, where the inner core was also allowed to tilt, was studied by Xu *et al.* (2000).

Incorporation of the combined effects of gravitational torque and viscous deformation of the inner core into a numerical geodynamo calculation was done by Buffett and Glatzmaier (2000), who demonstrated that the gravitational torque can significantly suppress inner-core rotation.

8.10.8 Summary

The inner core remains a difficult part of our planet to study. In every way it presents challenges: for mineral physicists, the extreme pressures and temperatures are difficult to achieve; for seismologists, the 5200 km of material above obfuscates inner-core signals; for geodynamicists, the wide variety and interaction of possible phenomena and the large uncertainty of physical parameters complicates interpretation. Nevertheless progress continues along multiple fronts: observational scientists will become yet better at extracting signals; experimentalists will continue to make technical improvements to achieve the extreme conditions of the inner core, and to design appropriate analog experiments; computational scientists will go where experimentalists cannot; and theoreticians will make progress in coupling data from all disciplines. Further progress towards understanding the inner core will require a multi- and interdisciplinary effort. We also hope and predict that geodynamicists will stimulate new observations, such as was the case with inner-core superrotation. Perhaps it should have been possible to have predicted inner-core elastic anisotropy prior to its discovery! Proposition of testable models by geodynamicists is one of the key directions to the study of the inner core.

It is always dangerous to make specific predictions about the directions a field of study will take, but we will nevertheless try. The composition of the light elements of the core is likely to remain uncertain–there are too many ways to put the puzzle together. This means that the phase diagram of the core will also remain uncertain. It does not mean, however, that there will be no progress toward understanding such important issues as the partitioning of elements between the inner and outer cores, and the light elements' effects on the melting temperature. On the other hand, it seems reasonable that we will make progress towards understanding the stable phases(s) of pure and alloyed iron under inner-core conditions. Likewise, we expect that the current uncertainty concerning the elastic constants of h.c.p. iron under inner-core conditions will get sorted out. Similarly, if there is another stable phase of iron in the inner core, we will determine its elastic properties.

Inner-core seismology is difficult, but hopefully not intractable. Over time we will come to some agreement concerning the elastic and anelastic properties of the inner core. Of particular interest will

be the geographic distributions of the elastic anisotropy, the bulk attenuation, and the attenuation anisotropy. One thing seems certain: as we get a better picture of the inner core, it, like the rest of the earth above, is not simple and featureless. In some ways this makes it less interesting – there is no one simple physical mechanism that can explain all the data. Ultimately, though, it shows that the inner core too exhibits the rich array of phenomena that makes earth science challenging and interesting. We predict that geodynamicists will take up the challenge to cross disciplines, and come to understand the origin of inner core anisotropy, in all of its detail as well as other interesting seismic properties that we dig up. We also predict that the inner core may hold some of the keys to understanding long-standing problems in the earth sciences, such as magnetic field generation and reversal, and core thermodynamics.

References

Alfe D, Price GD, and Gillan MJ (1999) Oxygen in the Earth's core: A first-principles study. *Physics of the Earth and Planetary Interiors* 110: 191–210.

Alfe D, Gillan MJ, and Price GD (2000) Constraints on the composition of the Earth's core from *ab initio* calculations. *Nature* 405: 172–175.

Anderson DL (1983) A new look at the inner core of the Earth. *Nature* 302: 660.

Anderson WW and Ahrens T (1996) Shock temperatures and melting in iron sulfides at core pressures. *Journal of Geophysical Research* 101: 5627–5642.

Aurnou JM, Brito D, and Olson PL (1996) Mechanics of inner core super-rotation. *Geophysical Research Letters* 23: 3401–3404.

Aurnou JM, Brito D, and Olson PL (1998) Anomalous rotation of the inner core and the toroidal magnetic field. *Journal of Geophysical Research* 103: 9721–9738.

Aurnou J and Olson P (2000) Control of inner core rotation by electromagnetic, gravitational and mechanical torques. *Physics of the Earth and Planetary Interiors* 117: 111–121.

Beghein C and Trampert J (2003) Robust normal mode constraints on inner-core anisotropy from model space search. *Science* 299: 552–555.

Belonoshko AB, Ahuja R, and Johansson B (2003) Stability of the body-centered-cubic phase of iron in the Earth's inner core. *Nature* 424: 1032–1034.

Bergman MI (1997) Measurements of elastic anisotropy due to solidification texturing and the implications for the Earth's inner core. *Nature* 389: 60–63.

Bergman MI (1998) Estimates of the Earth's inner core grain size. *Geophysical Research Letters* 25: 1593–1596.

Bergman MI (2003) Solification of the Earth's core. In: Veronique D, Kenneth C, Stephan Z, and Shun-Ichiro K (eds.) *Geodynamics Series, 31: Earth's Core: Dynamics, Structure, Rotation*, pp. 105–127, (10.1029/31GD08), Washington, DC: American Geophysical Union.

Bergman MI, Agrawal S, Carter M, and Macleod-Silberstein M (2003) Transverse solidification textures in hexagonal close-packed alloys. *Journal of Crystal Growth* 255: 204–211.

Bergman MI, Giersch L, Hinczewski M, and Izzo V (2000) Elastic and attenuation anisotropy in directionally solidified (hcp) zinc and the seismic anisotropy in the Earth's inner core. *Physics of the Earth and Planetary Interiors* 117: 139–151.

Bergman MI, Macleod-Silberstein M, Haskel M, Chandler B, and Akpan N (2005) A laboratory model for solidification of Earth's core. *Physics of the Earth and Planetary Interiors* 153: 150–164.

Birch F (1952) Elasticity and constitution of the Earth's interior. *Journal of Geophysical Research* 57: 227–286.

Boehler R (1992) Melting of the Fe–FeO and Fe–FeS systems at high pressures: Constraints on core temperatures. *Earth and Planetary Science Letters* 111: 217–227.

Boehler R (1996a) Fe–FeS eutectic temperatures to 620 kbar. *Physics of the Earth and Planetary Interiors* 96: 181–186.

Boehler R (1996b) Melting temperature of the Earth's mantle and core: Earth's thermal structure. *Annual Reviews – Earth and Planatery Sciences* 24: 15–40.

Bridgman PW (1949) Linear compression to 30,000 kg/cm^2, including relatively incompressible substances. *Proceedings of the American Academy of Arts and Sciences* 77: 187–234.

Brito D, Elbert D, and Olson P (2002) Experimental crystallization of gallium: Ultrasonic measurements of elastic anisotropy and implications for the inner core. *Physics of the Earth and Planetary Interiors* 129: 325–346.

Brown H and Patterson C (1948) The composition of meteoritic matter. III-Phase equilibria, genetic relationships, and planet structures. *Journal of Geology* 56: 85–111.

Buchwald VF (1975) *Handbook of Iron Meteorites,* Vol. 1: Berkeley CA: University of California Press.

Buffett BA (1996a) Gravitational oscillations in the length of day. *Geophysical Research Letters* 23: 2279–2282.

Buffett BA (1996b) A mechanism for decade fluctuations in the length of day. *Geophysical Research Letters* 23: 3803–3806.

Buffett BA (1997) Geodynamic estimates of the viscosity of the Earth's inner core. *Nature* 388: 571–573.

Buffett BA and Bloxham J (2000) Deformation of Earth's inner core by electromagnetic forces. *Geophysical Research Letters* 27: 4001–4004.

Buffett BA and Glatzmaier GA (2000) Gravitational braking of inner-core rotation in geodynamo simulations. *Geophysical Research Letters* 27: 3125–3128.

Buffett BA and Wenk H-R (2001) Texturing of the Earth's inner core by Maxwell stresses. *Nature* 413: 60–63.

Bullard EC (1950) The transfer of heat from the core of the Earth. *Monthly Notices of the Royal Astronomical Society* 6: 36–41.

Bullen KE (1949) Compressibility–pressure hypothesis and the Earth's interior. *Monthly Notices of the Royal Astronomical Society. Geophysical Supplement* 5: 355–368.

Cao A and Romanowicz B (2004) Hemispherical transition of seismic attenuation at the top of the Earth's inner core. *Earth and Planetary Science Letters* 228: 243–253.

Christensen UR and Tilgner A (2004) Power requirement of the geodynamo from Ohmic losses in numerical and laboratory dynamos. *Nature* 429: 169–171.

Cormier VF (1981) Short-period PKP phase and the anelastic mechanism of the inner core. *Physics of the Earth and Planetary Interiors* 24: 291–301.

Cormier VF, Li X, and Choy GL (1998) Seismic attenuation of the inner core: Viscoelastic or stratigraphic? *Geophysical Research Letters* 25: 4019–4022.

Cormier VF and Li X (2002) Frequency-dependent seismic attenuation in the inner core 2. A scattering and fabric interpretation. *Journal of Geophysical Research* 107(B12): 2362 (doi:10.1029/2002JB001796).

Creager KC (1992) Anisotropy of the inner core from differential travel times of the phases PKP and PKIKP. *Nature* 356: 309–314.
Creager KC (1997) Inner core rotation rate from small-scale heterogeneity and time-varying travel times. *Science* 278: 1284–1288.
Creager KC (1999) Large-scale variations in inner-core anisotropy. *Journal of Geophysical Research* 104: 23127–23139.
Creager KC (2000) Inner core anisotropy and rotation. In: Karato S-I, Stixrude L, Lieberman R, *et al.* (eds.) *Mineral Physics and Seismic Tomography From the Atomic to Global Scale*, pp. 89–114. Washington, DC: American Geophysical Union.
Cummins P and Johnson LR (1988) Synthetic seismograms for an inner core transition of finite thickness. *Geophysical Journal* 94: 21–34.
Doombos DJ (1983) Observable effects of the seismic absorption band in the Earth. *Geophysical Journal of the Royal Astronomical Society* 75: 693–11.
Dziewonski AM and Anderson DL (1981) Preliminary reference Earth model. *Physics of the Earth and Planetary Interiors* 25: 297–356.
Esbensen KH and Buchwald VF (1982) Planet (oid) core crystallization and fractionation-evidence from the Agpalilik mass of the Cape York iron meteorite shower. *Physics of the Earth and Planetary Interiors* 29: 218–232.
Fearn DR, Loper DE, and Roberts PH (1981) Structure of the Earth's inner core. *Nature* 292: 232–233.
Frost HH and Ashby MF (1982) *Deformation Mechanism Maps*. 166 pp. Tarrytown, NY: Pergamon.
Fukai Y (1984) The iron–water reaction and the evolution of the Earth. *Nature* 308: 174–75.
Gannarelli CM, Alfe S, and Gillan MJ (2003) The particle-in-cell model for ab initio thermodynamics: Implications for the elastic anisotropy of the Earth's inner core. *Physics of the Earth and Planetary Interiors* 139: 243–253.
Gessmann CK and Wood BJ (2002) Potassium in the Earth's core? *Earth and Planetary Science Letters* 200: 63–78.
Glatzmaier GA and Roberts PH (1995a) A three-dimensional self-consistent computer simulation of a geomagnetic field reversal. *Nature* 377: 203.
Glatzmaier GA and Roberts PH (1995b) A three-dimensional convective dynamo solution with rotating and finitely conducting inner core and mantle. *Physics of the Earth and Planetary Interiors* 91: 63.
Glatzmaier GA and Roberts PH (1996) Rotation and magnetism of the Earth's inner core. *Science* 274: 1887–1891.
Gubbins D (1981) Rotation of the inner core. *Journal of Geophysical Research* 86: 11695–11699.
Gubbins D, Masters TG, and Jacobs JA (1979) Thermal evolution of the Earth's core. *Geophysical Journal of the Royal Astronomical Society* 59: 57–99.
Haack H and Scott ERD (1992) Asteroid core crystallization by inward dendritic growth. *Journal of Geophysical Research* 97: 14727–14734.
Helffrich G, Kaneshima S, and Kendall J-M (2002) A local, crossing-path study of attenuation and anisotropy of the inner core. *Geophysical Research Letters* 29(12): 1568 (doi: 10.1029/2001GL014059).
Helffrich G and Kaneshima S (2004) Seismological constraints on core composition from Fe-O-S liquid immiscibility. *Science* 306: 2239–2242.
Ishii M and Dziewonski AM (2002) The innermost inner core of the Earth: Evidence for a change in anisotropic behavior at the radius of about 300 km. *Proceedings of the National Academy of Sciences* 99(22): 14026–14030.
Ishii M and Dziewonski AM (2003) Distinct seismic anisotropy at the center of the Earth. *Physics of the Earths and Planetary Interiors* 140: 203–217.
Jackson I, Fitzgerald JD, and Kokkonen H (2000) High temperature viscoelastic relaxation in iron and its implication for the shear modulus and attenuation of the Earth's inner core. *Journal of Geophysical Research* 105: 23605–23634.
Jackson KA (1958) Mechanism of growth. In: Maddin R, *et al.* (ed.) *Liquid Metals and Solidification*, pp. 174–186. Cleveland: American Society for Metals.
Jeanloz R (1990) The nature of the Earth's core. *Annual Review of Earth and Planetary Sciences* 18: 357–386.
Jeanloz R and Wenk H-R (1988) Convection and anisotropy of the inner core. *Geophysical Research Letters* 15: 72–75.
Jephcoat A and Olson P (1987) Is the inner core of the Earth pure iron? *Nature* 325: 332–335.
Kamb WB (1959) Theory of preferred crystal orientation developed by crystallization under stress. *Journal of Geology* 67: 153–170.
Kaneshima S, Hirahara K, Ohtaki T, and Yoshida Y (1994) Seismic structure near the inner core-outer core boundary. *Geophysical Research Letters* 21(2): 157–160.
Karato S (1993) Inner core anisotropy due to the magnetic field induced preferred orientation of iron. *Science* 262: 1708–1711.
Karato S (1999) Seismic anisotropy of the Earth's inner core resulting from flow induced by Maxwell stresses. *Nature* 402: 871–873.
Kubo A, Ito E, and Katsura T, *et al.* (2003) *In situ* X-ray observation of iron using Kawai-type apparatus equipped with sintered diamond: Absence of β phase up to 44 GPa and 2100 K. *Geophysical Research Letters* 30: 1126 (doi: 10.1029/2002GL016394).
Labrosse S, Poirier J-P, and Le Mouel J-L (2001) The age of the inner core. *Earth and Planetary Science Letters* 190: 111–123.
Laio A, Bernard S, Chiarotti GL, Scandolo S, and Tosatti E (2000) Physics of iron at Earth's core conditions. *Science* 287: 1027–1030.
Laske G and Masters G (1999) Rotation of the inner core from a new analysis of free oscillations. *Nature* 402: 66–69.
Leyton F, Koper KD, Zhu L, and Dombrovskaya M (2005) On the lack of seismic discontinuities in the inner core. *Geophysical Journal International* 162: 779–786.
Legrand B (1984) Relations entre la structure el′ectronique et la facilite de glissement dans les metaux hexagonaux compacts. *Philosophical magazine* 49: 171–184.
Li J and Agee CB (2001) Element partitioning constraints on the light element composition of the Earth's core. *Geophysical Research Letters* 28: 81–84.
Lin J-F, Heinz DL, Campbell AJ, Devine JM, and Shen G (2002) Iron–silicon alloy in Earth's core? *Science* 295: 313–315.
Lin J-F, Sturhahn W, Zhao J, Shen G, Mao H-K, and Hemley RJ (2005) Sound velocities of hot dense iron: Brich's law revisited. *Science* 308: 1892–1894.
Loper DE (1983) Structure of the inner core boundary. *Geophysical and Astrophysical Fluid Dynamics* 22: 139–155.
Loper DE and Fearn DR (1983) A seismic model of a partially molten inner core. *Journal of Geophysical Research* 88: 1235–1242.
Loper DE and Roberts PH (1978) On the motion of an iron-alloy core containing a slurry I. General theory. *Geophysical and Astrophysical Fluid Dynamics* 9: 289–321.
Loper DE and Roberts PH (1980) On the motion of an iron-alloy core containing a slurry II. A simple model. *Geophysical and Astrophysical Fluid Dynamics* 16: 83–127.
Loper DE and Roberts PH (1981) A study of conditions at the inner core boundary of the Earth. *Physics of the Earth and Planetary Interiors* 24: 302–307.
MacDonald GJF and Knopoff L (1958) The chemical composition of the outer core. *Journal of Geophysics* 1: 1751–1756.

Mao HK, Shu J, Shen G, Hemley RJ, Li B, and Singh AK (1998) Elasticity and rheology of iron above 220 GPa and the nature of the Earth's inner core. *Nature* 396: 741–743.
Mao HK, Shu J, Shen G, Hemley RJ, Li B, and Singh AK (1999) correction Elasticity and rheology of iron above 220 GPa and the nature of the Earth's inner core. *Nature* 399: 280.
Mason B (1966) Composition of the Earth. *Nature* 211: 616–618.
Masters TG and Shearer PM (1990) Summary of seismological constraints on the structure of the Earth's core. *Journal of Geophysical Research* 95: 21691–21695.
Matsui M and Anderson OL (1997) The case for a body-centered cubic phase (α') for iron at inner core conditions. *Physics of the Earth and Planetary Interiors* 103: 55–62.
Mavko G, Mukerji T, and Dvorkin J (1998) *The Rock Physics Handbook*. Cambridge: Cambridge University Press.
McDonough WF (2003) Compositional model for the Earth's core. In: Holland HD and Turekian KK (eds.) *Treatise on Geochemistry, vol. 2: The Mantle and core*, pp. 547–568. Oxford: Pergamon.
McElhinny MW and Senanayake WE (1980) Paleomagnetic evidence for the existence of the geomagnetic field 3.5 Ga ago. *Journal of Geophysical Research* 85: 3523–3528.
McQueen RG and Marsh SP (1966) Shock-wave compression of iron–nickel alloys and the earth's core. *Journal of Geophysical Research* 71: 1751–1756.
Miller WA and Chadwick GA (1969) The equilibrium shapes of small liquid droplets in solid-liquid phase mixtures: Metallic h.c.p. and metalloid systems. *Proceedings of the Royal society of London Series A* 312: 257–276.
Morse SA (1986) Adcumulus growth of the inner core. *Geophysical Research Letters* 13: 1557–1560.
Morse SA (2002) No mushy zones in the Earth's core. *Geochimica et cosmochimica Acta* 66(12): 2155–2165.
Mullins WW and Sekerka RF (1963) Morphological stability of a particle growing by diffusion or heat flow. *Journal of Applied Physics* 34: 323–329.
Mullins WW and Sekerka RF (1964) Stability of a planar interface during solidification of a dilute binary alloy. *Journal of Applied Physics* 35: 444–451.
Murthy VR and Hall HT (1970) The chemical composition of the Earth's core: Possibility of sulfur in the core. *Physics of the Earth and Planetary Interiors* 2: 276–282.
Murthy VR, van Westrenen W, and Fei Y (2003) Experimental evidence that potassium is a substantial radioactive heat source in planetary cores. *Nature* 423: 163–165.
Niu F and Wen L (2001) Hemispherical variations in seismic velocity at the top of the Earth's inner core. *Nature* 410: 1081–1084.
Okuchi T (1997) Hydrogen partitioning into molten iron at high pressures: Implications for Earth's core. *Science* 278: 1781–1784.
Oreshin SI and Vinnik LP (2004) Heterogeneity and anisotropy of seismic attenuation in the inner core. *Geophysical Research Letters* 31: L02613 (doi:10.1029/2003GL018591).
Poirier J-P (1985) *Creep of Crystals*. New York: Cambridge University Press.
Poirier J-P (1994) Light elements in Earth's outer core; A critical review. *Physics of the Earth and Planetary Interiors* 85: 319–337.
Poirier J-P and Price GD (1999) Primary slip system of epsilon-iron and anisotropy of the Earth's inner core. *Physics of the Earth and Planetary Interiors* 110: 147–156.
Porter DA and Easterling KE (1992) *Phase Transformations in Metals and Alloys*. London: Chapman and Hall.
Poupinet G and Kennett BLN (2004) On the observation of high frequency PKiKP and its coda in Australia. *Physics of the Earth and Planetary Interiors* 146: 497–511.
Ringwood AE (1977) Composition of the core and implications for the origin of the Earth. *Geochemical Journal* 11: 111–135.
Ringwood AE and Hibberson W (1990) The system Fe–FeO revisited. *Physics and Chemistry Minerals* 17: 313–319.
Rochester MG (1962) Geomagnetic core–mantle coupling. *Journal of Geophysical Research* 67: 4833–4836.
Ross M, Young DA, and Grover R (1990) Theory of the iron phase diagram at Earth core conditions. *Journal of Geophysical Research* 95: 21713–21716.
Rutter JW (1958) Imperfections resulting from solidification. In: Maddin R, *et al.* (eds.) *Liquid Metals and Solidification*, pp. 243–262. Cleveland: American Society for Metals.
Sanloup C and Fei Y (2004) Closure of the Fe–S–Si liquid miscibility gap at high pressure. *Physics of the Earth and Planetary Interiors* 147: 57–65.
Sayers CM (1989) Seismic anisotropy of the inner core. *Geophysical Research Letters* 16: 270–276.
Saxena SK, Shen G, and Lazor P (1993) Experimental evidence for a new iron phase and implications for Earth's core. *Science* 260: 1312–1314.
Shanker J, Singh BP, and Srivastava SK (2004) Volume–temperature relationship for iron at 330 GPa and the Earth's core density deficit. *Physics of the Earth and Planetary Interiors* 147: 333–341.
Sherman DM (1995) Stability of possible Fe-FeS and Fe-FeO alloy phases at high pressure and the composition of the Earth's core. *Earth and Planetary Science Letters* 132: 87–98.
Shimizu H, Poirier J-P, and Le Mouel J-L (2005) On crystallization at the inner core boundary. *Physics of the Earth and Planetary Interiors* 151: 37–51.
Singh SC, Taylor MAJ, and Montagner J-P (2000) On the presence of liquid in Earth's inner core. *Science* 287: 2471–2474.
Söderlind P, Moriarty JA, and Wills JM (1996) First-principles theory of iron up to Earth-core pressures: Structural, vibrational and elastic properties. *Physical Review B-condensed Matter* 53: 14063–14072.
Song X and Helmberger DV (1992) Velocity structure near the inner core boundary from waveform modeling. *Journal of Geophysical Research* 97(B5): 6573–6586.
Song X and Helmberger DV (1993) Anisotropy of the Earth's inner core. *Geophysical Research Letters* 20: 285–288.
Song X and Helmberger DV (1995) A P wave velocity model of Earth's core. *Journal of Geophysical Research* 100(B7): 9817–9830.
Song XD and Helmberger DV (1998) Seismic evidence for an inner core transition zone. *Science* 282: 924–927.
Song XD and Richards PG (1996) Observational evidence for differential rotation of the Earth's inner core. *Nature* 382: 221–224.
Souriau A and Poupinet G (1991) The velocity profile at the base of the liquid core from PKP(BC+Cdiff) data: An argument in favour of radial inhomogeneity. *Geophysical Research Letters* 18(11): 2023–2026.
Souriau A and Poupinet G (2003) Inner core rotation: A critical appraisal. In: Dehant V, *et al.* (eds.) *Geodynamics Series, vol. 31: Earth's Core: Dynamics, Structure, Rotation*, pp. 65–82, (10.1029/31GD06), Washington, DC: AGU.
Souriau A and Roudil P (1995) Attenuation in the uppermost inner core from broad-band GEOSCOPE PKP data. *Geophysical Journal International* 123: 572–587.
Souriau A and Romanowicz B (1996) Anisotropy in inner core attenuation: A new type of data to constrain the nature of the solid core. *Geophysical Research Letters* 23(1): 1–4.
Souriau A and Romanowicz B (1997) Anisotropy in the inner core: Relation between P-velocity and attenuation. *Physics of the Earth and Planetary Interiors* 101: 33–47.
Spetzler H and Anderson DL (1968) The effect of temperature and partial melting on velocity and attenuation in a simple binary system. *Journal of Geophysical Research* 73: 6051–6060.

Stacey FD (1992) *Physics of the Earth,* 3rd edn. Brisbane: Brookfield Press.

Steinle-Neumann G, Stixrude L, and Cohen RE (1999) First-principles elastic constants for the hcp transition metals Fe, Co and Re at high pressure. *Physical Review B* 60: 791–799.

Steinle-Neumann G, Stixrude L, Cohen RE, and Gulseren O (2001) Elasticity of iron at the temperature of the Earth's inner core. *Nature* 413: 57–60.

Steinle-Neumann G, Stixrude L, and Cohen RE (2003) Physical properties of iron in the inner core. In: Dehant V, *et al.* (eds.) Geodynamics Series, 31: *Earth's Core: Dynamics, Structure, Rotation,* pp. 213–232, (10.1029/31GD10), Washington, DC: AUG.

Stevenson DJ (1983) Anomalous bulk viscosity of two-phase fluids and implications for planetary interiors. *Journal of Geophysical Research* 88(B3): 2445–2455.

Stixrude L and Cohen RE (1995) High-pressure elasticity of iron and anisotropy of the Earth's inner core. *Science* 267: 1972–1975.

Stixrude L, Wasserman E, and Cohen RE (1997) Composition and temperature of Earth's inner core. *Journal of Geophysical Research* 102: 24729–24739.

Stocker RL and Gordon RB (1975) Velocity and internal friction in partial melts. *Journal of Geophysical Research* 80: 4828–4836.

Su WJ, Dziewonski AM, and Jeanloz R (1996) Planet within a planet: Rotation of the inner core. *Science* 274: 1883–1887.

Sumita I and Olson P (1999) A laboratory model for convection in Earth's core driven by a thermally heterogeneous mantle. *Science* 286: 1547–1549.

Sumita I and Olson P (2002) Rotating thermal convection experiments in a hemispherical shell with heterogeneous boundary heat flux: Implications for the Earth's core. *Journal of Geophysical Research* 107: 10.1029/2001JB000548.

Sumita I and Yoshida S (2003) Thermal interactions between the mantle, outer and inner cores, and the resulting structural evolution of the core. In: Dehant V, Kenneth C, Shun-Ichiro K, *et al.* (eds.) *Geodynamics Series, 31: Earth's Core: Dynamics, Structure, Rotation* pp. 213–232 and (10.1029/31GD14), Washington: AGU.

Sumita I, Yoshida S, Hamano Y, and Kumazawa M (1995) A model for the structural evolution of the Earth's core and its relation to the observations. In: Yu kutake T (ed.) *The Earth's Central Part: Its Structure and Dynamics*, pp. 231–261. Toyko: Terra Scientific.

Sumita I, Yoshida S, Kumazawa M, and Hamano Y (1996) A model for sedimentary compaction of a viscous medium and its application to inner-core growth. *Geophysical Journal International* 124: 502–524.

Tait S, Jahrling K, and Jaupart C (1992) The planform of compositional convection and chimney formation in a mushy layer. *Nature* 359: 406–408.

Tanaka S and Hamaguchi H (1997) Degree one heterogeniety and hemispherical variation of anisotropy in the inner core from PKP(BC)–PKP(DF) times. *Journal of Geophysical Research* 102: 2925–2938.

Tanaka S and Hamaguchi H (1993) Degree one heterogeniety at the top of the Earth's core, revealed by SmKS Travel Times. In: Le Mouel JL, *et al.* (ed.) *Geophysical Monograph Series, 72: Dynamics of the Earth's Deep Interior and Earth Rotation*, pp. 127–134. Washington: IUGG and AUG.

Van Orman JA (2004) On the viscosity and creep mechanism of Earth's inner core. *Geophysical Research Letters* 31: L20606 (doi: 10.1029/2004GL021209).

Vidale JE and Earle PS (2000) Fine-scale heterogeneity in the Earth's inner core. *Nature* 404: 273–275.

Vidale JE, Dodge DA, and Earle PS (2000) Slow differential rotation of the Earth's inner core indicated by temporal changes in scattering. *Nature* 405: 445–448.

Vocadlo L, Brodholt J, Alfe D, Price GD, and Gillan MJ (1999) The structure of iron under the conditions of the Earth's inner core. *Geophysical Research Letters* 26: 1231–1234.

Vocadlo L, Alfe D, Gillan MJ, Wood IG, Brodholt JP, and Price GD (2003) Possible thermal and chemical stabilization of body-centered-cubic iron in the Earth's core. *Nature* 424: 536–539.

Wang JN, Wu JS, and Ding Y (2002) On the transitions among different creep regimes. *Materials Science and Engineering A* 334: 275–279.

Watanabe T and Kurita K (1994) Simultaneous measurements of the compressional-wave velocity and the electrical conductivity in a partially molten material. *Journal of Physics of the Earth* 42: 69–87.

Weber P and Machetel P (1992) Convection within the inner-core and thermal implications. *Geophysical Research Letters* 19: 2107–2110.

Weeks WF and Wettlaufer JS (1996) Crystal orientations in floating ice sheets. In: Arsenault RJ, Cole D, Gross T, *et al.* (eds.) *The Johannes Weertman Symposium*, pp. 337–350. Zimbabwe: The Minerals, Metals, & Materials Society.

Wen L and Niu F (2002) Seismic velocity and attenuation structures in the top of the Earth's inner core. *Journal of Geophysical Research* 107B11: 2273 (doi: 10.1029/2001JB000170).

Wenk H-R, Baumgardner JR, Lebenson RA, and Tome CN (2000a) A convection model to explain anisotropy of the inner core. *Journal of Geophysical Research* 105: 5663–5677.

Wenk H-R, Matthies S, Hemley RJ, Mao H-K, and Shu J (2000b) The plastic deformation of iron at pressures of the Earth's inner core. *Nature* 405: 1044–1047.

Wenk H-R, Takeshita T, Jeanloz R, and Johnson GC (1988) Development of texture and elastic anisotropy during deformation of hcp metals. *Geophysical Research Letters* 15: 76–79.

Widmer R, Masters G, and Gilbert F (1991) Spherically symmetric attenuation within the Earth from normal mode data. *Geophysical Journal International* 104: 541–553.

Wood BJ (1993) Carbon in the core. *Earth and Planetary Science Letters* 117: 593–607.

Xu S, Crossley D, and Szeto AMK (2000) Variations in length of day and inner core differential rotation from gravitational coupling. *Physics of the Earth and Planetary Interiors* 117: 95–110.

Yoshida S, Sumita I, and Kumazawa M (1996) Growth model of the inner core coupled with outer core dynamics and the resulting elastic anisotropy. *Journal of Geophysical Research* 101: 28085–28103.

Yu W and Wen L (2006) Inner core attenuation anisotropy. *Earth and Planetary Science Letters* 245: 581–594.

Yukutake T (1998) Implausibility of convection in the Earth's inner core. *Physics of the Earth and Planetary Interiors* 108: 1–13.

Zhang J, Song X-D, Li Y, Richards PG, Sun X, and Waldhauser F (2005) Inner core differential motion confirmed by earthquake waveform doublets. *Science* 309: 1357–1360.